Volume 4
Number 14
21 July 2022
Pages 2953–3112

Nanoscale Advances

rsc.li/nanoscale-advances

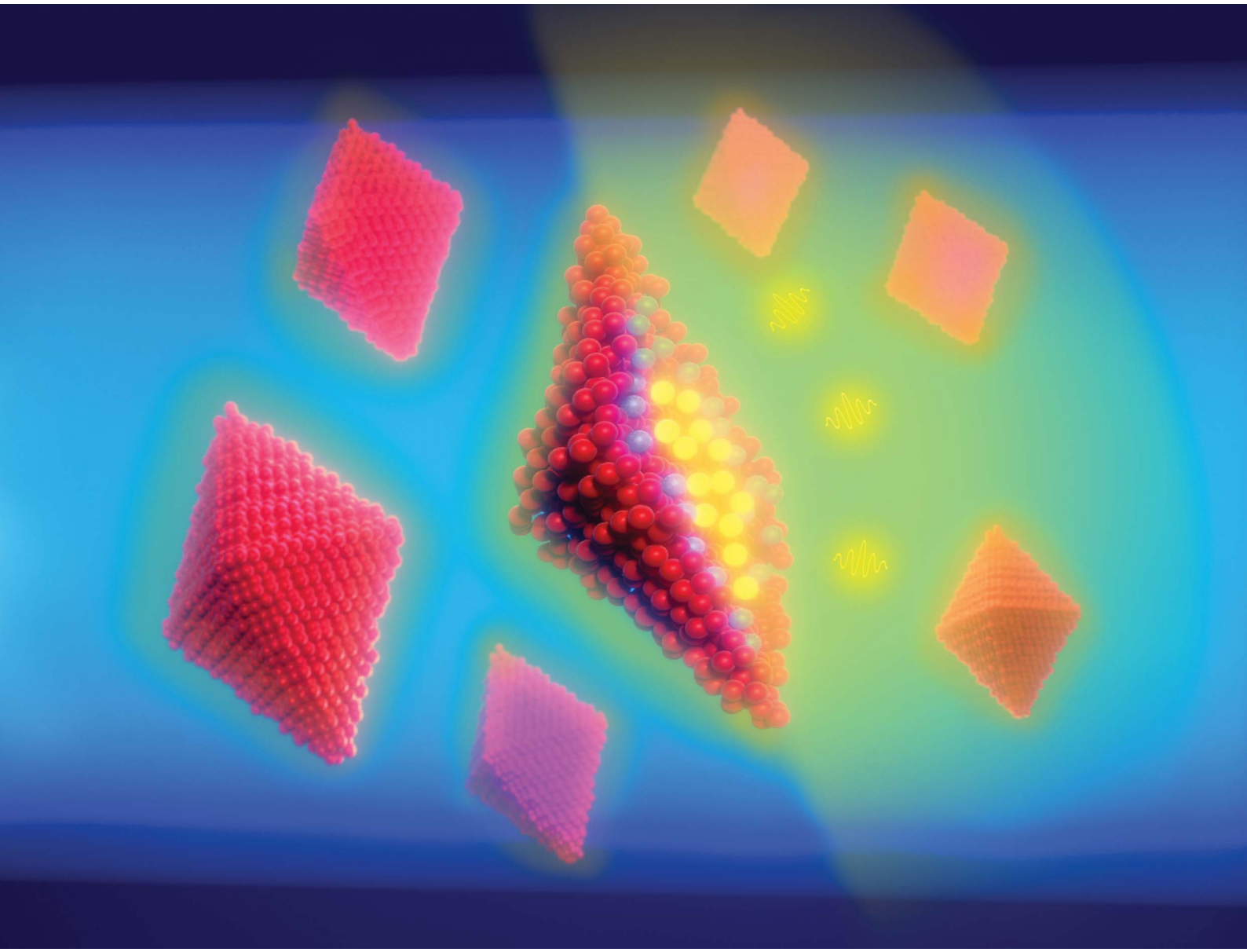

ISSN 2516-0230

ROYAL SOCIETY OF CHEMISTRY

COMMUNICATION

Rajesh Komban, Simon Spelthann, Christoph Gimmler *et al.*
Bulk-like emission in the visible spectrum of colloidal $LiYF_4$:Pr nanocrystals downsized to 10 nm

NCNST

Nanoscale Advances

ROYAL SOCIETY OF CHEMISTRY

COMMUNICATION

View Article Online
View Journal | View Issue

Cite this: *Nanoscale Adv.*, 2022, **4**, 2973

Received 19th January 2022
Accepted 20th April 2022

DOI: 10.1039/d2na00045h

rsc.li/nanoscale-advances

Bulk-like emission in the visible spectrum of colloidal $LiYF_4$:Pr nanocrystals downsized to 10 nm†

Rajesh Komban, ‡*[a] Simon Spelthann, ‡*[b] Michael Steinke, [b] Detlev Ristau, [bcd] Axel Ruehl,[c] Christoph Gimmler *[a] and Horst Weller [ae]

Though Pr^{3+} doped $LiYF_4$ ($LiYF_4$:Pr^{3+}) bulk crystals are a well-known laser gain material with several radiative transitions, their nanocrystal counterparts have not been investigated with regards to these. Through downsizing to the nanoscale, novel applications are expected, especially in composite photonic devices. For example, nanocrystals in stable colloidal form with narrow size distribution are highly desirable to reduce scattering in such composites. Herein, we synthesized monodispersed $LiYF_4$:Pr^{3+} nanocrystals having a size of 10 nm resulting in colorless clear stable colloidal dispersions and conducted an extensive optical characterization for the first time. We observed unexpected yet intense emission with excited state lifetimes comparable to bulk crystals in the visible spectrum through excitation at 444 nm and 479 nm. In macroscopic bulk crystals, this emission is only exploitable through excitation of a different, subjacent energy level. A comprehensive comparison to the bulk crystals provides deeper insight into the excitation mechanism and performance of these nanocrystals. The presented results pave the way for developing application-oriented $LiYF_4$:Pr^{3+} nanocrystals as emitters with tailored properties for quantum optics or biomedical applications.

Just like sodium rare earth tetrafluorides ($NaREF_4$; where RE = Y, Gd, Lu), their lithium counterparts, $LiREF_4$, are considered ideal host lattices due to their low phonon frequency when compared to oxides, phosphates, oxysulphides, and vanadates.[1] For example, Haase, Güdel, and their co-workers demonstrated an efficiency increase of the upconversion luminescence in $NaREF_4$ compared to rare earth phosphate.[2] This, and the possible exploitation of radiation in the visible spectrum, are the main reasons why upconversion $LiREF_4$ nanocrystals have been investigated profusely and found to be promising for life science, photovoltaic and sensing applications.[3] However, visible transitions in upconversion nanocrystals based on $NaREF_4$ and $LiREF_4$ show quite low quantum yield. Even if they are provided with an inert shell to reduce quenching, the quantum yield is lower than 10%.[4]

Generation of photons in the visible spectrum has attracted a large number of researchers within several areas of optical applications. For instance, organic dyes are applied as fluorescence marker in microscopy.[5] Furthermore, semiconductor quantum dots are used in display technology[6] or as single photon sources[7] while light sources based on nonlinear effects can be exploited in spectroscopy as in the present work. Compared to previously mentioned options, generating visible photons using lanthanide ions offers high long-term stability, robustness against environmental conditions, and excellent spectroscopic properties. Among the lanthanides, Pr^{3+} shows intense emissions from the vacuum ultraviolet up to near infrared spectral regions, which found application in laser physics,[8] phosphors,[3j,9] or microscopy.[10]

Most of these applications require not only excellent spectroscopic properties but also high optical-to-optical efficiencies which cannot be obtained with upconversion nanocrystals due to their low quantum yield. To evaluate the potential for such applications, the optical properties of Pr^{3+} doped $NaREF_4$ have been characterized.[9b,c] However, high quantum yields of Pr^{3+} doped $NaREF_4$ nanocrystals were not reported yet, to the best of our knowledge. A striking fact is that the respective crystal structures of Na and Li based rare earth tetrafluorides are very different: while for $NaREF_4$ the cubic and hexagonal crystal phases dominate, $LiREF_4$ exists only in tetragonal form. However, it is the tetragonal host lattice that reveals novel and

[a]*Fraunhofer Center for Applied Nanotechnology CAN – (A Research Division of Fraunhofer Institute for Applied Polymer Research, 14476 Potsdam, Germany), Grindelallee 117, 20146 Hamburg, Germany. E-mail: rajesh.komban@iap.fraunhofer.de; christoph.gimmler@iap.fraunhofer.de*

[b]*Leibniz University Hannover, Institute of Quantum Optics, Welfengarten 1, 30167 Hannover, Germany. E-mail: spelthann@iqo.uni-hannover.de*

[c]*Leibniz University Hannover, QUEST-Leibniz-Research School, Institute of Quantum Optics, Callinstraße 36, 30167 Hannover, Germany*

[d]*Cluster of Excellence PhoenixD (Photonics, Optics and Engineering – Innovation Across Disciplines), Germany*

[e]*University of Hamburg, Department of Chemistry, Grindelallee 117, 20146 Hamburg, Germany*

† Electronic supplementary information (ESI) available. See https://doi.org/10.1039/d2na00045h

‡ Authors contributed equally to this work.

important possibilities such as quantum cutting properties, *e.g.* of Eu^{3+} doped $LiGdF_4$ bulk crystals with a quantum efficiency of nearly 200%.[11]

Downsizing of tetragonal Pr^{3+}doped $LiREF_4$ to the nanoscale is an interesting path to reduce scattering in photonic composite media. Moreover, the available literature on $LiYF_4$:-Pr^{3+} nano- and microparticles specifies the necessity of developing high quality nanoparticles of these materials as they are polydisperse with a size above 30 nm.[12] On the other hand, syntheses of $LiYF_4$ upconversion nanocrystals co-doped with Yb^{3+}, Er^{3+}, Tm^{3+}, and Ho^{3+} have been reported by different groups,[3] and size tuning as well as core@shell nanostructures have also been demonstrated by some of them. The syntheses reported include a simple one pot synthesis method: rare earths chlorides in presence of oleic acid are heated, forming oleates *in situ*, which avoids a separate synthesis of precursor materials.[3i] In the case of Pr^{3+} doped $LiYF_4$ however, we observed a lattice disintegration into tri-fluoride as evident from the XRD and TEM data provided in the ESI (Fig. S1†). Additionally, by changing the amount of oleic acid, a polydisperse size distribution was observed as well as presence of other phases (refer Fig. S2†). We concluded that the right amount of oleic acid, in combination with right heating temperature and heating duration to form *in situ*-oleates are all playing a crucial role to obtain high quality $LiYF_4$:Pr^{3+} nanocrystals.

Of another concern is a yellowish/brownish coloration of the reaction mixture during heat-up in an oleic acid-based synthesis, which imparts coloration of the purified particles too. Often we witnessed it even inert atmosphere was assured during the heating. Though a detailed study of this effect is out of scope of this work, we speculate on oxidation of other fatty acids present in the oleic acid or formation of more complex structures among those in presence of oxygen at higher temperatures. This may not be a big concern in the case of upconversion nanoparticles as they are excited in the NIR region. However, as our goal is to produce high quality $LiYF_4$:-Pr^{3+} nanocrystals, which are being excited in the blue spectrum, the optical properties would suffer significantly due to unwanted absorption and loss of transparency. This concern is justified by a simple experiment where we measure absorption and emission spectra of slightly (left for several hours at room temperature) and strongly (heated to 300 °C for 4 h) colored oleic acid containing $LiYF_4$:Pr^{3+} nanocrystals as shown in Fig. 1. The colored solutions exhibit strong absorption at short wavelengths, expanding towards longer wavelengths. When exciting such a sample, respective emission lines appear in the visible spectrum and intensify for strongly colored oleic acid. In improperly synthesized $LiYF_4$:Pr^{3+} nanocrystal dispersions, the characteristic absorption and emission lines of the Pr^{3+} ions and colorized oleic acid are superimposed, thus distorting the optical properties of the Pr^{3+} emission.

We have found how to handle these problems and developed high quality $LiYF_4$:Pr^{3+} nanocrystals having an average size of 10 nm, which allowed us to conduct a detailed spectroscopic characterization for the first time. Details on the synthesis method are provided in the ESI.† Compared to macroscopic bulk crystals, the nanocrystalline counterparts show a strongly

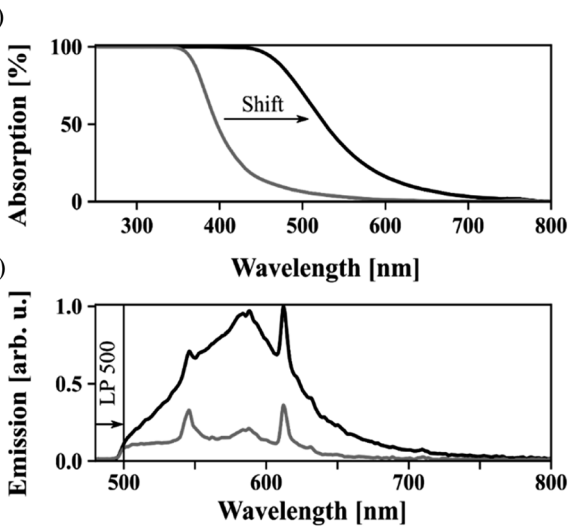

Fig. 1 Absorption (a) and emission (b) of strongly (black) and lightly (grey) colorized oleic acids.

broadened absorption, and we developed a novel fitting method to quantify the spectral broadening. Most interestingly, the nanocrystals exhibit an additional strong emission line at 595 nm from the intermediate $^1D_2$ energy level when excited between 444 nm and 479 nm. In bulk crystals, emission from this level only occurs through excitation between 575 nm and 600 nm. However, the lifetime of the intermediate $^1D_2$ level in the nanocrystals is well comparable to the bulk crystals' lifetime. We infer that the understanding of the emission mechanism presented here further offers an additional degree of freedom for tuning the spectroscopic properties to a specific application.

Since the optimum doping concentration of Pr^{3+} ions in the nanocrystals depends on the particle size and correlations have not yet been thoroughly studied, we have chosen four Pr^{3+}concentrations, 0.65, 1, 1.3, and 1.5 at%, for doping the $LiYF_4$ nanocrystals. The range of these values include the optimum doping concentration of 0.65 at% reported for bulk crystals, which is mainly limited by concentration quenching.[8b] Due to the strong impact of surface ions in nanocrystals, the concentration quenching is expected to be lower and hence the projected optimum doping concentration is somewhat larger compared to the bulk case. The actual Pr^{3+} ions concentration in the nanocrystals was analyzed using EDX coupled to a high-resolution TEM and results are provided in Table 1. The corresponding mean values are 0.7, 1.05, 1.14, and 1.47%,

Table 1 EDX data

Samples	Targeted, at%	Analyzed, at%
$LiYF_4$:Pr (0.7)	0.65	0.7
$LiYF_4$:Pr (1.05)	1.0	1.05
$LiYF_4$:Pr (1.14)	1.3	1.14
$LiYF_4$:Pr (1.47)	1.5	1.47

respectively, and are in good agreement with the targeted doping concentrations. For discussion of the results, we have used the doping concentration values found by EDX analysis.

TEM measurements of the $LiYF_4:Pr^{3+}$ nanocrystals together with corresponding size distributions and photographs of dispersions containing these nanocrystals are shown in Fig. 2. Well-defined individual nanocrystals having a size of around 10 nm are clearly evident in the respective TEM analysis (Fig. 2a–d). The tetragonal crystal structure of these nanocrystals is confirmed by the XRD analysis as reflections agree well with those of bulk $LiYF_4$ (PDF # 01-081-1940), see Fig. S3.† Furthermore, mapping and line scan (see ESI Fig. S4a and b†) analysis indicates that the doping was successful as the homogeneous distribution of Pr ions in the nanocrystals is evident.

Though these are small sized nanocrystals of only 10 nm, their tetragonal bipyramidal shape is visible and some high resolution TEM images are also provided in Fig. S5† for further proof. This shape is easily recognizable in larger crystals (refer Fig. S5†), however, depending on the viewing angle and the particles' alignment on the TEM grid, their shape can easily be mistaken for diamond or hexagonal morphologies as described in publications on $LiYF_4$ nanocrystals doped with other lanthanideions.[3j] Size distributions of the $LiYF_4:Pr^{3+}$ nanocrystals were determined and are shown in Fig. 2e–h. The mean size of the edges are $(8.74 \pm 0.64) \times (10.39 \pm 0.7)$ nm, $(10.3 \pm 0.66) \times (12.42 \pm 0.86)$ nm, $(10.95 \pm 0.87) \times (13.17 \pm 0.84)$ nm, and $(9.58 \pm 0.72) \times (11.78 \pm 1.07)$ nm for nanocrystals with increasing doping concentrations. A direct relation between the doping concentration and the nanocrystal size is not evident. Actually, using an appropriate amount of oleic acid in the reaction mixture effectively controls the size distribution and provides a stable dispersion without any visible sedimentation even after several months of storing. The high quality of our developed nanocrystals is supported by the photographs of the individual dispersions as these samples are colorless and transparent, see Fig. 2i–l, which show no precipitation or turbidity.

To demonstrate the versatility of our synthesis, we furthermore synthesized nanocrystals tuned in size with consistently narrow size distribution at higher doping level of 5%. The sizes and distributions for $LiYF_4$ nanocrystals doped with 5% Pr^{3+}, which have an average size of 10 to 20 nm, are provided in the histogram in Fig. 3, and representative TEM pictures of 15 and 20 nm sized particles can be found in the ESI (Fig. S6†). In this work, however, we restrict ourselves to the low doped nanocrystals.

We performed a detailed spectroscopic characterization of the 10 nm sized nanocrystals and compared their properties to the bulk crystals' properties as reported in the literature.[8,13a,b] The absorption cross section spectra of the 1.47 at% doped nanocrystals and those of all four samples are provided in Fig. 4a and S7,† respectively. We found that the peak absorption cross sections differ by three orders of magnitude with respect to the cross section of bulk crystals. While bulk crystals exhibit a peak absorption cross section of up to 1.7×10^{-19} cm^2 at 444 nm, the nanocrystals' is 3.4×10^{-22} cm^2. At the same time, the spectral linewidths are strongly broadened and shifted compared to their bulk counterparts. Thus, instead of comparing the peak values, the integrated cross sections should be compared, which only yield a differential factor of 45. While the absorption lines of bulk crystals are well described by Lorentzian profiles, see Fig. S8,† the corresponding transitions in nanocrystals deviate from this line shape.

To quantify this effect, we utilized a novel fitting approach that only requires a few fit parameter to easily determine line shape deviations and the nature of spectral broadening. For this method, the weighted sum of the bulk crystal spectra for every crystal axis is convolved with a single Voigt profile and fitted to the nanocrystal data (refer ESI† for further details). The fit resulted in a shift of the bulk spectra of around $\Delta\lambda = 2$ nm, and

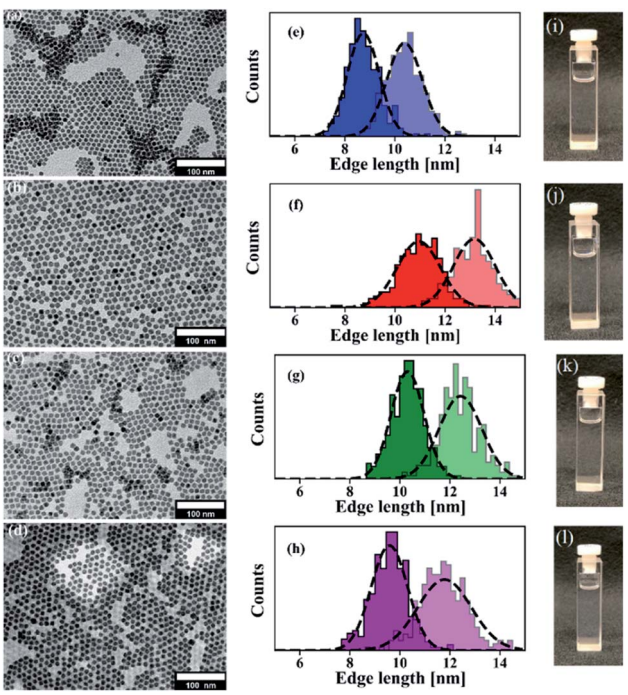

Fig. 2 TEM analysis of $LiYF_4:Pr^{3+}$ nanocrystals with varying Pr^{3+} concentration: (a) 0.7, (b) 1.05, (c) 1.14, and (d) 1,47 at%. Corresponding particle size distributions (e–h) and photographs of colloidal dispersions in toluene (i–l).

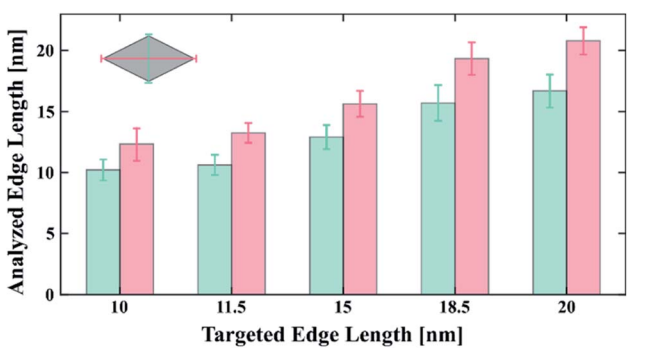

Fig. 3 Size distributions of $LiYF_4:Pr^{3+}$ nanocrystals with 5% Pr^{3+} concentration from 10 to 20 nm.

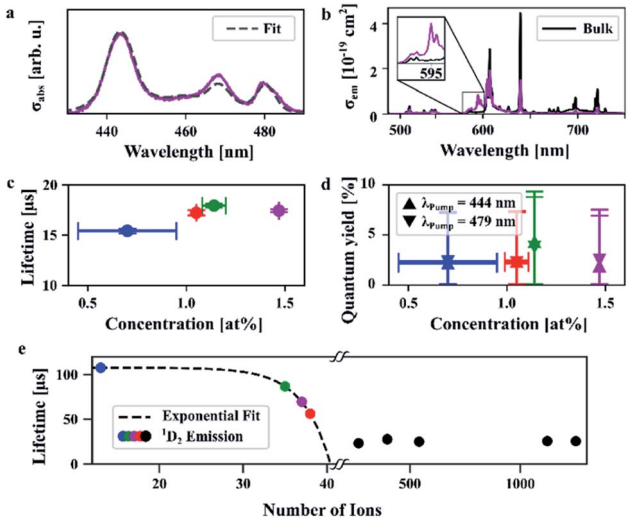

Fig. 4 Spectroscopic results: (a) absorption cross sections and fit from bulk spectra of the 1.47 at% doped nanocrystals. The other samples yielded comparable results but are not depicted here for reasons of clarity, see Fig. S6.† (b) Emission cross sections of the 1.47 at% doped nanocrystals in comparison to bulk crystals. (c) Lifetimes and (d) quantum yield for two different excitation wavelengths. (e) The lifetime of the $^1D_2$ level decreases with the number of ions within the nanocrystals.

the ratio of the bulk spectra was fitted to be around 0.3 to 0.4, which means that around 2/3 of the absorption originates from the two *a*-axes and around 1/3 from the *c*-axis as expected due to the random orientation of the nanocrystals in the organic solvent. The Voigt profile contained mainly the Gaussian component with a full width at half maximum (FWHM) of 4–6 nm. A non-broadened component was allowed in the fit, too, which was, however, less than 2% of the broadened spectrum and thus considered neglectable.

The Gaussian nature of the broadening of the absorption spectra indicates an inhomogeneous broadening mechanism. From the observed spectral shift, it can be inferred that the field of the surrounding medium has a strong influence on the Pr^{3+} ions, which results in the inhomogeneous broadening. Assuming a nearly uniform distribution of Pr^{3+} ions, significantly more ions are located at the surface than within the nanocrystal's volume due to its high surface-to-volume ratio as already known from the literature.[3j,8c] The ratio of the non-broadened component is indeed small (<2%), but non-zero. Therefore, it can be deduced that only a small number of ions are not influenced by the field of the surrounding medium.

We excited the nanocrystals at either 444 nm or 479 nm to investigate their spontaneous emission behaviour in the visible spectrum. In Fig. 4b the emission cross sections of nanocrystals (1.47 at%) and bulk crystals excited at 444 nm are provided, which are of a comparable order of magnitude. Emission cross sections of all four samples and that of bulk crystals being based on each of the different crystal axes (*a* and *c*) are given in Fig. S9 and S10,† respectively. Bulk crystals exhibit peak emission cross sections of up to 2.2×10^{-19} cm^2 at an emission wavelength of 640 nm. A similar value of 1.9×10^{-19} cm^2 was obtained for the nanocrystals, albeit at another transition, at 607 nm. At 640 nm, however, the emission cross section of nanocrystals is about three times smaller than for the bulk crystals, similar to what was found for the absorption.

The emission spectra show neither broadening nor spectral shifts, which is unexpected since a comparable behaviour for emission and absorption spectra is predicted by McCumber theory.[14] However, at this size scale, mainly the ions in the center of the nanocrystal contribute to the emission. In contrast, surface ions of the nanocrystals experience not only the crystal field but also the field of the surrounding medium. This effect causes a transition from the excited $^3P_0$ to the lower energy $^1D_2$ level *via* multi-phonon quenching (MPQ). The un-broadened emission spectra indicate that, obviously, MPQ has a greater characteristic length scale than the local field effect which causes the spectrally broadened absorption. It follows that ions potentially contributing to a broadened emission spectrum lose their energy due to MPQ.

We further observe a strong emission line at 595 nm which corresponds to a transition from the $^1D_2$ level and is evident in the nanocrystals' spectra, compare inset in Fig. 4b. Although populating the $^1D_2$ level *via* reabsorption of the $^1P_0$ emission at 604 nm and 607 nm is in principle possible, this effect is estimated to be very weak due to the low respective absorption cross sections. We infer that, thus, MPQ leads to a significant population of the $^1D_2$ level. The $^1D_2$ level does not only emit at 595 nm but in a broad spectral range from 570 nm to 610 nm. Within this spectral range, $^3P_0$ emission takes place as well, which means that the emission in this particular range is a superposition of $^1D_2$ and $^3P_0$ emissions. This superposition shifts the spectral position of the peak emission cross section from 607 nm in bulk crystals to 640 nm in the nanocrystals. The ratio between emission at 640 nm and 595 nm can be used to estimate the nanocrystal's correct emission cross sections in the spectral region of superposition and is calculated to be 0.6×10^{-19} cm^2 at 607 nm.

The measured excited state lifetimes of the $^3P_0$ level range between 15 and 18 µs as evident from Fig. 4c. Richter and co-workers reported a lifetime of 35.7 µs for bulk crystal doped with 0.65 at%.[8b] Here, the 0.7% doped nanocrystals show an experimentally determined quantum yield of 3.2% and a lifetime of 15.4 ± 0.2 µs (see ESI† for experimental details on both measurements), which is about 40% of the radiative lifetime in bulk crystals (Fig. 4d). From that, one would expect either a somewhat higher quantum yield or a lower radiative lifetime, as high lifetimes are associated with well suppressed non-radiative transitions resulting in high quantum yields. In case of the nanocrystals, however, the strong MPQ of the surface ions increases the nonradiative rates, which we estimate to be around 20–50 times higher than the radiative rates, refer the ESI.† The surface ions' contribution to the spontaneous emission is thus suppressed so that ions in the center reveal emission properties comparable to bulk crystals.

The measured excited state lifetimes of the $^1D_2$ level populated *via* MPQ are surprisingly high. For the 0.7% and 1.14% doped nanocrystals the lifetimes of 108 µs and 87 µs are well comparable to bulk lifetimes from that level which are 101 µs

and 66 μs, respectively.[8i] We found that the lifetimes of the nanocrystals decrease exponentially with the number of Pr^{3+} ions as depicted in Fig. 4e. To confirm that this behavior is no size effect we measured the $^1D_2$ decay from $LiYF_4$:Pr^{3+} nanocrystals with sizes ranging from 10 to 20 nm and significantly more than 50 ions per nanocrystal. The resulting lifetimes were determined to be around 25 ± 2 μs and showed no dependence to the nanocrystals' size or number of ions as inferred from Fig. 4e. From that, we conclude that cross relaxations drive the $^1D_2$ depopulation. The mechanism starts with two adjacent ions which are in states ($^1D_2$, $^3H_4$), respectively, and exchange energy so that their final states are ($^1G_4$, $^3F_4$), compare the dashed lines in Fig. S11.†[8c] Altogether, we find that the visible emission originating from the $^1D_2$ level is not quenched in our 10 nm $LiYF_4$:Pr^{3+} nanocrystals compared to bulk $LiYF_4$:Pr^{3+} single crystals. This makes our nanocrystals an interesting candidate for application in nanocrystal composite laser gain media or quantum memories operating in the visible spectrum.[15]

Conclusions

In conclusion, we successfully developed a synthesis procedure of stable colloidal nanocrystals of $LiYF_4$:Pr^{3+} with an average size of 10 nm and monodisperse size distribution for the first time. This procedure enables a precise size control preserving a narrow size distribution of $LiYF_4$:Pr^{3+} nanocrystals. We performed a comprehensive spectroscopic analysis and developed a novel yet simple method to quantify the nanocrystals' spectral broadening and shifts. We compared the nanocrystals' spectroscopic behaviour to macroscopic bulk crystals and observed strong multi-phonon quenching, which results in reduced quantum yields. This effect is indeed disadvantageous for visible emission from the ^{3}P-manifold. At the same time, the multi-phonon quenching efficiently populates the $^1D_2$ state, which yields strong emission at 595 nm. We found that the excited state lifetime of this transition is limited by cross relaxations and is comparable to bulk crystals for small nanocrystals with low doping concentration. The understanding of the efficient population process of the $^1D_2$ level allows for an additional degree of freedom during the design of $LiYF_4$:Pr^{3+} nanocrystals for photonic applications like phosphors, quantum optics, and biomedical applications.

Author contributions

C. G., D. R., H. W., and A. R. led the collaboration efforts and supervised the project. R. K. and S. S. conceived the idea and initiated the project. R. K. designed the synthesis. R. K. and C. G. were involved in characterization of nanocrystals. S. S. and A. R. designed the spectroscopic experiments, carried out the spectroscopic measurements, analysis and interpretation of the data. M. S. was involved in fitting procedure for the absorption spectra and its interpretation. A. R. designed the spectroscopic figure-of-merit and contributed to the interpretation of data. R. K. and S. S. wrote the manuscript, which was revised by C. G., A. R., M. S., H. W., and D. R. All authors participated in the discussion and processing of the manuscript.

Conflicts of interest

There are no conflicts of interest to declare.

Acknowledgements

R. K., C. G. and H. W. would like to thank Free and Hanseatic City of Hamburg, Germany for the financial support. The work of S. S., M. S., A. R. and D. R. was partly funded by: Deutsche Forschungsgemeinschaft (DFG, German Research Foundation) under Germany's Excellence Strategy – EXC-2123 Quantum Frontiers – 390837967. D. R. would like to thank the Deutsche Forschungsgemeinschaft (DFG, German Research Foundation) for partly funding this work under Germany's Excellence Strategy within the Cluster of Excellence PhoenixD (EXC 2122, Project ID 390833453). The publication of this article was funded by the Open Access Fund of the Leibniz Universität Hannover. Dr Michael Zopf, Institute of Solid State Physics at Leibniz University Hannover, Germany helped with the fitting procedure of multi-exponential decays. Pascal Rusch, Institute of Physical Chemistry and Electrochemistry at Leibniz University Hannover, Germany performed the quantum yield measurement. Dr Christian Kraenkel, Leibniz-Institut für Kristallzüchtung Berlin, Germany provided absorption and emission cross section data for $LiYF_4$:Pr bulk crystals. The authors also thank Ms Andrea Koeppen and Mr Stefan Werner, University of Hamburg (UHH), Germany for their supports for the microscopic and XRD analyses. Special thanks go to Mr Andreas Kornowski, a long-term collaborator and expert in the field of electron microscopy of nanoscopic materials at UHH. His contribution by material characterization greatly helped in shaping this publication. Unfortunately, he passed away before this paper could be submitted/published.

References

1 (*a*) G. Chen, H. Qiu, P. N. Prasad and X. Chen, *Chem. Rev.*, 2014, **114**, 5161; (*b*) R. Alia, S. M. Saleha, R. J. Meiera, H. A. Azabb, I. I. Abdelgawadc and O. S. Wolfbeis, *Sens. Actuators, B*, 2010, **150**, 126; (*c*) C. Liu, Z. Wang, H. Jiaa and Z. Li, *Chem. Commun.*, 2011, **47**, 4661.

2 (*a*) S. Heer, O. Lehmann, M. Haase and H.-U. Güdel, *Angew. Chem., Int. Ed.*, 2003, **42**, 3179; (*b*) S. Heer, K. Kömpe, H.-U. Güdel and M. Haase, *Adv. Mater.*, 2004, **16**, 2102.

3 (*a*) P. Huang, W. Zheng, S. Zhou, D. Tu, Z. Chen, H. Zhu, R. Li, E. Ma, M. Huang and X. Chen, *Angew. Chem., Int. Ed.*, 2014, **53**, 1252; (*b*) J. Shin, J.-H. Kyhm, A.-R. Hong, J. D. Song, K. Lee, H. Ko and H. S. Jang, *Chem. Mater.*, 2018, **30**, 8457; (*c*) M. S. Meijer, P. A. Rojas-Gutierrez, D. Busko, I. A. Howard, F. Frenzel, C. Würth, U. Resch-Genger, B. S. Richards, A. Turshatov, J. A. Capobianco and S. Bonnet, *Phys. Chem. Chem. Phys.*, 2018, **20**, 22556; (*d*) Q. Ju, U. Uddayasankar and U. Krull, *Small*, 2014, **10**, 3912; (*e*) V. Mahalingam, F. Vetrone, R. Naccache, A. Speghini and J. A. Capobianco, *Adv. Mater.*, 2009, **21**, 4025; (*f*) F. Carl, L. Brink, M. Pons, C. Würth, U. Resch-Genger and M. Haase, *Nano Res.*, 2021, **14**, 797; (*g*) T. Cheng, R. Marin,

A. Skripka and F. Vetrone, *J. Am. Chem. Soc.*, 2018, **140**, 12890; (*h*) Y.-P. Du, Y.-W. Zhang, L.-D. Sun and C.-H. Yan, *Dalton Trans.*, 2009, 8574; (*i*) F. Wang, J. Wang, Y. Xu, Y. Wang, Y. Liu, X. Chen, H. Chen and X. Liu, *C. R. Chim.*, 2010, **13**, 731; (*j*) S. Y. Kim, J. S. Jeong, K. A. Mkhoyan and H. S. Jang, *Nanoscale*, 2016, **8**, 10049.

4 (*a*) P. Lei, R. An, X. Zhai, S. Yao, L. Dong, X. Xu, K. Du, M. Zhang, J. Feng and H. Zhang, *J. Mater. Chem. C*, 2017, **5**, 9659; (*b*) G. Chen, T. Y. Ohulchanskyy, A. Kachynski, H. Agren and P. N. Prasad, *ACS Nano*, 2011, **5**, 4981; (*c*) J.-C. Boyer and C. J. M. van Veggel, *Nanoscale*, 2010, **2**, 1417; (*d*) A. N. Generalova, V. V. Rocheva, A. V. Nechaev, D. A. Khochenkov, N. V. Sholina, V. A. Semchishen, V. P. Zubov, A. V. Koroleva, B. N. Chichkov and E. V. Khaydukov, *RSC Adv.*, 2016, **6**, 30089.

5 W. J. Lichtman and J.-A. Conchello, *Nat. Methods*, 2005, **2**, 910.

6 (*a*) T.-H. Kim, K.-S. Cho, E. K. Lee, J. Chae, J. W. Kim, D. H. Kim, J.-Y. Kwon, G. Amaratunga, S. Y. Lee, B. L. Choi, Y. Kuk, J. M. Kim and K. Kim, *Nat. Photonics*, 2011, **5**, 176; (*b*) J. Kim, H. J. Shim, J. Yang, M. K. Choi, D. C. Kim, J. Kim, T. Hyeon and D.-H. Kim, *Adv. Mater.*, 2017, **29**, 1700217; (*c*) H. Moon, C. Lee, W. Lee, J. Kim and H. Chae, *Adv. Mater.*, 2019, **31**, 1804294; (*d*) J. Y. Yang, M. K. Choi, U. J. Yang, S. Y. Kim, Y. S. Kim, J. H. Kim, D.-H. Kim and T. Hyeon, *Nano Lett.*, 2021, **21**(1), 26.

7 (*a*) R. Keil, M. Zopf, Y. Chen, B. Höfer, J. Zhang, F. Ding and O. G. Schmidt, *Nat. Commun.*, 2017, **8**, 15501; (*b*) M. Zopf, T. Macha, R. Keil, E. Urunuela, Y. Chen, W. Alt, L. Ratschbacher, F. Ding, D. Meschede and O. G. Schmidt, *Phys. Rev. B*, 2018, **98**, 161305(R).

8 (*a*) A. Richter, E. Heumann, E. Osiac, G. Huber, W. Seelert and A. Diening, *Opt. Lett.*, 2004, **29**, 2638; (*b*) A. Richter, E. Heumann, G. Huber, V. Ostroumov and W. Seelert, *Opt. Express*, 2007, **15**, 5172; (*c*) A. Richter, *Laser parameters and performance of Pr^{3+}-doped fluorides operating in the visible spectral region*, Cuvillier Verlag, Göttingen, Niedersachsen, Deutschland, 1st edn, 2007; (*d*) N.-O. Hansen, A.-R. Bellancourt, U. Weichmann and G. Huber, *Appl. Opt.*, 2010, **49**, 3864; (*e*) P. W. Metz, F. Reichert, F. Moglia, S. Müller, D.-T. Marzahl, C. Kraenkel and G. Huber, *Opt. Lett.*, 2014, **39**, 3193; (*f*) W. Bolanos, G. Brasse, F. Starecki, A. Braud, J.-L. Doualan, R. Moncorgé and P. Camy, *Opt. Lett.*, 2014, **39**, 4450; (*g*) M. Gaponenko, P. W. Metz, A. Härkönen, A. Heuer, T. Leinonen, M. Guina, T. Südmeyer, G. Huber and C. Kraenkel, *Opt. Lett.*, 2014, **39**, 6939; (*h*) C. Kraenkel, D. T. Marzahl, F. Moglia, G. Huber and P. W. Metz, *Laser Photonics Rev.*, 2016, **10**, 548; (*i*) P. Wu, B. Xiao, Q. Feng, X. Lin, W. Li, H. Xu and Z. Cai, *J. Lumin.*, 2021, **235**, 118028.

9 (*a*) S. Espinoza, M.-F. Volhard, H. Kätker, H. Jenneboer, A. Uckelmann, M. Haase, M. Müller, M. Purschke and T. Jüstel, *Part. Part. Syst. Charact.*, 2018, **35**, 1800282; (*b*) B. Herden, J. Nordmann, R. Komban, M. Haase and T. Jüstel, *Opt. Mater.*, 2013, **35**, 2062; (*c*) M. A. Gusowski, H. C. Swart, L. S. Karlsson and M. Trzebiatowska-Gusowska, *Nanoscale*, 2012, **4**, 541.

10 (*a*) D. Rieländer, K. Kutluer, P. M. Ledingham, M. Gündogan, J. Fekete, M. Mazzera and H. Riedmatten, *Phys. Rev. Lett.*, 2014, **112**, 040504; (*b*) T. Utikal, E. Eichhammer, L. Petersen, A. Renn, S. Götzinger and V. Sandoghdar, *Nat. Commun.*, 2014, **5**, 3627; (*c*) K. Xia, R. Klesov, Y. Wang, P. Siyushev, T. Kornher, R. Reuter, S. Yang and J. Wrachtrup, *New J. Phys.*, 2020, **22**, 073002.

11 R. T. Wegh, H. Donker, K. D. Oskam and A. Meijerink, *Science*, 1999, **283**, 663.

12 (*a*) M. Pudovkin, S. Korableva, D. Koryakovtseva, E. Lukinova, A. Lovchev, O. Morozov and V. Semashko, *J. Nanopart. Res.*, 2019, **21**, 266; (*b*) M. Pudovkin, S. Korableva, E. Lukinova, D. Koryakovtseva, O. Morozov and V. Semashko, *EPJ Web Conf.*, 2019, **220**, 02011.

13 (*a*) L. Esterowitz, F. J. Bartoli and R. E. Allen, *Phys. Rev. B: Condens. Matter Mater. Phys.*, 1979, **19**, 6442; (*b*) J. L. Adam, W. A. Silbey and D. R. Gabbe, *J. Lumin.*, 1985, **33**, 391.

14 D. E. McCumber, *Phys. Rev.*, 1964, **136**, A954.

15 T. Zhong and P. Goldner, *Nanophotonics*, 2019, **8**(11), 2003.